Vol 16 No 6, June 2007
1009-1963/2007/16(06)/1624-08

Chinese Physics

© 2007 Chin. Phys. Soc.
and IOP Publishing Ltd

A shaped annular beam tri-heterodyne confocal microscope with good anti-environmental interference capability*

Zhao Wei-Qian(赵维谦)[a)†], Feng Zheng-De(冯政德)[b)], and Qiu Li-Rong(邱丽荣)[a)]

[a)] *School of Information Engineering, Beijing Institute of Technology, Beijing* 10081, *China*

[b)] *Department of Automation Measurement and Control Engineering, Harbin Institute of Technology, Harbin* 150001, *China*

(Received 12 September 2006; revised manuscript received 27 December 2006)

A shaped annular beam tri-heterodyne confocal microscope has been proposed to improve the anti-environmental interference capability and the resolution of a confocal microscope. It simultaneously detects far-, on-, and near-focus signals with given phase differences by dividing the measured light path of the confocal microscope into three sub-paths (signals). Pair-wise real-time heterodyne subtraction of the three signals is used to improve the anti-environmental interference capability, axial resolution, and linearity; and a shaped annular beam super-resolution technique is used to improve lateral resolution. Theoretical analyses and preliminary experiments indicate that an axial resolution of about 1 nm can be achieved with a shaped annular beam tri-heterodyne confocal microscope and its lateral resolution can be better than 0.2 μm for $\lambda = 632.8$ nm, the numerical aperture of the lens of the microscope is NA = 0.85, and the normalized radius $\varepsilon = 0.5$.

Keywords: confocal microscopy, super-resolution, surface measurements
PACC: 0760P

1. Introduction

Confocal microscopes (CMs) are widely used for measurement of surface contours because their lateral resolutions are 1.4 times better than those of conventional microscopes.[1−6] The basic principle of differential confocal microscopy (DCM), based on confocal microscopy, is to use the slopes of a CM's axial response curves to measure the surface contours, and DCM has been used to achieve an axial resolution of 2 nm.[2] A confocal scanning optical microscope based on the DCM principle was proposed for surface topography measurement and analysis.[3,4] A fibre CM was proposed for the measurement of discontinuous grooves in compact discs.[5] However, (1) it is difficult to improve the anti-environmental interference capability of existing CM imaging systems because they directly use intensity signals, which are subject to the influence of various factors such as disturbances in intensity, the surrounding lighting, and the ambient temperature; (2) the diffractive effect makes the lateral resolution of a CM two orders of magnitude below its axial resolution, so the lateral and axial resolutions of the CM are not compatible with each other at all — its lateral resolution is about 0.4 μm only, whereas its axial resolution is on the nanometre level; and (3) the nonlinearity of a CM's axial intensity curve reduces the accuracy of the confocal microscopic measurement. It is difficult to use confocal microscopy to measure the dimensions of three-dimensional (3D) microstructures such as microsteps, microgrooves, and line-widths of integrated circuits. A lot of researches have therefore been conducted to improve the anti-environmental interference capability and the resolution of CMs.

A photoelectric detector with the same properties as those of a CM photoelectric detector has been used in a CM system to perform real-time measurement of the disturbance in the intensity of the light source and the normalization of the signal's intensity; thus, the effect of the disturbances can be suppressed.[2] However, this approach cannot be used to suppress the effect of such factors as variations in the reflectivity of the surface of the object, the surrounding lighting, and the ambient temperature and environmen-

*Project supported by the National Natural Science Foundation of China (Grant No 50475035), the Doctoral Program of Higher Education of China (Grant No 20050213035) and the Program for New Century Excellent Talents in University of China (Grant No NCET-05-0348).

†E-mail: zwq669@126.com

tal vibrations. A dual-receiving confocal light path arrangement and heterodyne subtraction of the signals received in a heterodyne receiving light path system were used in Ref.[7] to improve the axial resolution and anti-environmental interference capability, but the diffractive effect limited the lateral resolution to about 0.4 μm only.

The following measures have all been attempted to improve the resolution of CMs: a leaky annular pupil filter was used to improve the axial resolution of the CM;[8] a rectangular pupil filter was used to sharpen the lateral straight-edge response by as much as 2.36 times;[9] heterodyne subtraction of the signals received from two detectors of different sizes behind the collective lens of CMs was performed;[10] a super-resolution pupil filter[11−14] with continuous variation in phase and an annular transmission pupil filter were designed to improve the spatial resolution of CMs; a three-zone annular amplitude super-resolution pupil filter was designed to enable the point-spread function (PSF) to be compressed in the lateral direction and sharpened in the axial direction.[15] Two types of three-zone phase-only pupil filter were designed using both the axial and the lateral half-width at half-maximum (HWHM) of the PSF as the optimized object function to meet the super-resolution requirements.[16] However, when a single pupil filter is used to improve the spatial resolution of CMs, the improvement in spatial resolution is usually not obvious because the super-resolution must be achieved in both the lateral and axial directions simultaneously.

A shaped annular-beam tri-heterodyne confocal microscope (SATCM) is therefore proposed to improve the anti-environmental interference capability and spatial resolution of CMs. This approach is entirely different from those mentioned above. A SATCM detects far-, on-, and near-focus signals simultaneously with given phase differences by dividing the measured light path of the CM into three sub-paths (signals). Pair-wise real-time heterodyne subtraction of the three signals is used to improve the anti-environmental interference capability, axial resolution, and linearity; and a shaped annular beam super-resolution technique is used to improve the lateral resolution. The reduction in the axial resolution of the SATCM resulting from an incident shaped-annular-beam passing through the light path arrangement for pair-wise heterodyne subtraction can be simultaneously compensated.

2. SATCM imaging principle

As shown in Fig.1, the offset of a pinhole from the focal plane along the optical axis of a CM changes the axial intensity response phase of the CM; a SATCM uses this property to divide the receiving light path into three sub-paths which are focused by three collecting lenses of the same type. The three confocal photoelectric detecting systems consist of three sets of pinholes and detectors placed behind, at, and before the focus.

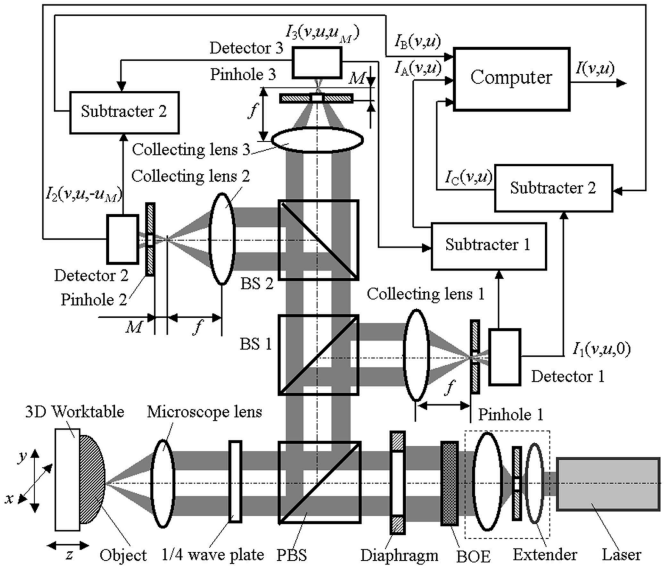


Fig.1. SATCM imaging principle.

A binary optical element (BOE) is used in a SATCM to improve its lateral resolution by shaping an incident Gaussian laser beam into an annular one and changing the spatial frequency distribution of the incident beam to reduce the size of the main lobe of the airy spot.

In a SATCM, the laser beam passes through an extender and a BOE and is shaped into an annular beam, which passes through an adjustable diaphragm and a polarized beam splitter (PBS), and is then converted into a p-light with its polarization direction parallel to the paper surface. The p-light passes through a 1/4 wave plate and is focused on the surface of the object by a microscope objective; the light used for measurement, together with the information reflected from the object, passes through the 1/4 wave plate again and is converted into an s-light with its polarization direction perpendicular to the surface of the paper. The s-light is reflected by the PBS onto the beam splitter 1 (BS1). Then the light used for measurement is split into two beams by BS1:One of them is reflected from the BS1 and focused by the collecting lens 1 to pass through pinhole 1, placed at the focus of the collecting lens 1, so that it can be received by detector 1. The other beam passing through BS1 is split by BS2 again into two beams; the beam used for measurement is reflected from BS2 and focused by the collecting lens 2 to pass through pinhole 2, located at a distance M from the focus of collecting lens 2, and is received by detector 2. The light passing through BS2 used for measurement is focused by collecting lens 3 to pass through pinhole 3, located at a distance M from collecting lens 3, and is received by detector 3. Heterodyne subtraction processing systems 1, 2, and 3 perform pairwise real-time heterodyne subtraction of the three signals simultaneously received with given phases; and the resulting signals are processed by a computer to achieve 3D super-resolution microscopic imaging detection. BS1 has a split beam ratio of 2:1 between transmission and reflection, and BS2 has a ratio of 1:1.

The intensity of the interference signal in a CM is affected by such factors as variation in the intensity of the light source, the reflectivity of the surface of the object, the surrounding lighting, the ambient temperature, and environmental vibrations; it is denoted E_i, where $i = 1, 2, 3$.

When an object is moved in the axial or lateral direction, the light source, extender, BOE, adjustable diaphragm, PBS, 1/4 wave plate, microscope lens, collecting lens 1, pinhole 1, and photoelectric detector 1 constitute a shaped annular beam CM, and the intensity response, $I_1(v, u, 0)$, received by photoelectric detector 1 is expressed as[17]

$$I_1(v,u,0) = \left| \left[2\int_{\varepsilon}^{1} (\exp(\mathrm{j}u\rho^2/2) J_0(\rho v)\rho/\sqrt{(1-\varepsilon^2)})\mathrm{d}\rho \right] \right|^2 \times \left| \left[2\int_{\varepsilon}^{1} (\exp(\mathrm{j}\rho^2 u/2) J_0(\rho v)\rho/\sqrt{(1-\varepsilon^2)})\mathrm{d}\rho \right] \right|^2 + E_1, \quad (1)$$

where J_0 is a first-order Bessel function, ρ is the normalized radial radius, u and v are axial and lateral normalized optical coordinates respectively, and ε is the ratio of the inner to the outer radius of an annular beam.

The light source, extender, BOE, adjustable diaphragm, PBS, 1/4 wave plate, microscope lens, collecting lens 2, pinhole 2, and photoelectric detector 2 form a shaped annular beam para-CM with a detector placed behind the focus, and the intensity response, $I_2(v, u, -u_M)$, received by photoelectric detector 2 is expressed as[17]

$$I_2(v,u,-u_M) = \left| \left[2\int_{\varepsilon}^{1} (\exp((\mathrm{j}u\rho^2)/2) J_0(\rho v)\rho/\sqrt{(1-\varepsilon^2)})\mathrm{d}\rho \right] \right|^2 \times \left| \left[2\int_{\varepsilon}^{1} (\exp(\mathrm{j}\rho^2(u-u_M)/2) J_0(\rho v)\rho/\sqrt{(1-\varepsilon^2)})\mathrm{d}\rho \right] \right|^2 + E_2, \quad (2)$$

where u_M is the value of the optical normalized coordinate corresponding to a distance M of the detector from the focus of a collecting lens in the axial direction.

The light source, extender, BOE, adjustable diaphragm, PBS, 1/4 wave plate, microscope lens, collecting lens 3, pinhole 3, and photoelectric detector 3 form a shaped annular beam para-CM with a detector placed

before the focus, and the intensity response, $I_3(v,u,+u_M)$, received by photoelectric detector 3 is expressed as[17]

$$I_3(v,u,+u_M) = \left| \left[2\int_{\varepsilon}^{1} (\exp(\mathrm{j}u\rho^2/2)J_0(\rho v)\rho/\sqrt{(1-\varepsilon^2)})\mathrm{d}\rho \right] \right|^2 \times \left| \left[2\int_{\varepsilon}^{1} (\exp(\mathrm{j}\rho^2(u+u_M)/2)J_0(\rho v)\rho/\sqrt{(1-\varepsilon^2)})\mathrm{d}\rho \right] \right|^2 + E_3. \quad (3)$$

The results of pair-wise heterodyne subtraction among the signals $I_1(v,u,0)$, $I_2(v,u,-u_M)$, and $I_3(v,u,+u_M)$ are

$$\begin{aligned} I_{\mathrm{A}}(v,u) &= I_1(v,u,0) - I_2(v,u,-u_M) + E_1 - E_2, \\ I_{\mathrm{B}}(v,u) &= I_1(v,u,0) - I_3(v,u,+u_M) + E_1 - E_3, \\ I_{\mathrm{C}}(v,u) &= I_2(v,u,-u_M) - I_3(v,u,+u_M) + E_2 - E_3. \end{aligned} \quad (4)$$

$I_1(v,u,0)$, $I_2(v,u,-u_M)$, and $I_3(v,u,+u_M)$ are the intensity signals simultaneously received in the three photoelectric detecting systems with the same properties, so that the corresponding intensity interference signals, E_1, E_2, and E_3, caused by such factors as variations in the intensity of the light source, the reflectivity of the surface of the object, the surrounding lighting, the ambient temperature, and environmental vibrations are almost the same. Thus, Eq.(4) can be simplified to

$$\begin{aligned} I_{\mathrm{A}}(v,u) &\approx I_1(v,u,0) - I_2(v,u,-u_M), \\ I_{\mathrm{B}}(v,u) &\approx I_1(v,u,0) - I_3(v,u,+u_M), \\ I_{\mathrm{C}}(v,u) &\approx I_2(v,u,-u_M) - I_3(v,u,+u_M). \end{aligned} \quad (5)$$

A computer is used to perform the real-time processing of $I_{\mathrm{A}}(v,u)$, $I_{\mathrm{B}}(v,u)$, and $I_{\mathrm{C}}(v,u)$, and the intensity response, $I(v,u)$, of the SATCM is given by

$$I(v,u) = \begin{cases} I_{\mathrm{A}}(v,u) & \text{if} \quad I_{\mathrm{C}}(v,u) \geq 0 \\ I_{\mathrm{B}}(v,u) & \text{if} \quad I_{\mathrm{C}}(v,u) < 0. \end{cases} \quad (6)$$

The magnitude of intensity response, $I(v,u)$, corresponds to the knaggy change of the object, and it is used to reconstruct the surface contour and microdimensions of the object. Figure 2(a) shows the normalized intensity response, $I(v,u)$, of the SATCM obtained using Eq.(6). Figure 2(b) shows the normalized intensity response, $I_1(v,u,0)$, of a conventional CM, and compared with $I_1(v,u,0)$, the main lobe of $I(v,u)$ is obviously sharpened, the linearity of $I(v,u)$ in the axial direction is significantly improved, and the side lobe of $I(v,u) \geq 0$ is obviously suppressed.

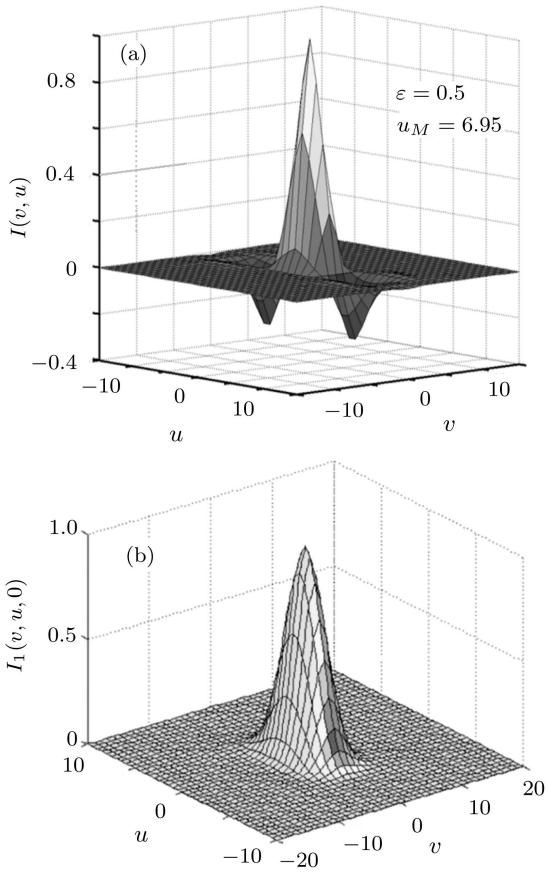


Fig.2. Normalized simulated curved surfaces of SATCM and CM intensities. (a) Intensity response of SATCM. (b) Intensity response of CM.

For given system parameters such as the numerical aperture of the microscope lens, the pinhole size, and the sensitivity of the detector, the sensitivities of the slopes of the linear intervals in the axial intensity curves $I_{\mathrm{A}}(0,u)$, $I_{\mathrm{B}}(0,u)$, and $I_{\mathrm{C}}(0,u)$ depend on u_M, and there exists a u_M that maximizes the slope in the linear interval of $I(0,u)$.

In Fig.3, the sensitivity $k_{\mathrm{A}}(0,u,u_M)$ is obtained using the differential of the heterodyne signal $I_{\mathrm{A}}(0,u)$ with respect to u, and the slopes $k_{\mathrm{A}}(0,u,u_M)$ and $k_{\mathrm{A}}(0,0,u_M)$ are equal in the linear interval, so that the slope of $I_{\mathrm{A}}(0,u)$ in the linear interval can be expressed as $k_{\mathrm{A}}(0,0,u_M)$,

$$k_{\mathrm{A}}(0,0,u_M) = (1-\varepsilon^2)^3 \cdot \sin c[u_M(1-\varepsilon^2)/4\pi] \times [\{u_M(1-\varepsilon^2)/4\} \cdot \cos\{u_M(1-\varepsilon^2)/4\} - \sin\{u_M(1-\varepsilon^2)/4\}]/\{u_M(1-\varepsilon^2)/4\}^2. \quad (7)$$

Similarly, the slope $k_{\mathrm{B}}(0,0,u_M)$ of $I_{\mathrm{B}}(0,u)$ in the linear interval in Fig.3 is

$$k_{\mathrm{B}}(0,0,u_M) = (1-\varepsilon^2)^3 \cdot \sin c[u_M(1-\varepsilon^2)/4\pi] \times [\{u_M(1-\varepsilon^2)/4\} \cdot \cos\{u_M(1-\varepsilon^2)/4\} - \sin\{u_M(1-\varepsilon^2)/4\}]/\{u_M(1-\varepsilon^2)/4\}. \quad (8)$$

The slope, $k_{\mathrm{C}}(0,0,u_M)$, of $I_{\mathrm{C}}(0,u)$ in the linear interval in Fig.3 is given by

$$k_{\mathrm{C}}(0,0,u_M) = -2 \times (1-\varepsilon^2)^3 \cdot \sin c[u_M(1-\varepsilon^2)/4\pi] \times [\{u_M(1-\varepsilon^2)/4\} \cdot \cos\{u_M(1-\varepsilon^2)/4\} - \sin\{u_M(1-\varepsilon^2)/4\}]/\{u_M(1-\varepsilon^2)/4\}^2. \quad (9)$$

When $\varepsilon = 0.5$, $u_M = \pm 6.95$, and the absolute values of $k_{\mathrm{A}}(0,0,u_M)$, $k_{\mathrm{B}}(0,0,u_M)$, and $k_{\mathrm{C}}(0,0,u_M)$, the extreme values obtained by calculating the extreme values of Eqs.(5), (6), and (7), are the largest (i.e. they are 0.15, 0.15, and 0.30, respectively). When $\varepsilon = 0.5$, the slopes of $I(v,0)$ and $I(0,u)$ are also the greatest in the bevel intervals.

The intensity curves $I_1(0,u,0)$, $I_2(0,u,-u_M)$, $I_3(0,u,+u_M)$, $I_{\mathrm{C}}(0,u)$, and $I(0,u)$ for $\varepsilon = 0.5$ and $u_M = \pm 6.95$ are shown in Fig.3(a), and their normalized axial curves are shown in Fig.3(b). The SATCM works in the range $I(0,u) \geq 0$ when it is used for imaging, and it is seen from Fig.3(b) that the slope in the bevel interval of $I(0,u) \geq 0$ is obviously larger than that of $I_1(0,u,0)$ in the measurement range. The linearity of the two bevel intervals in curve $I(0,u)$ is better than that in curve $I_1(0,u,0)$.

As shown in Fig.3, conventional CMs use the slope of the intensity response curve, $I_1(0,u,0)$, for measurement of the dimensions of 3D microstructures, and the accuracy of the measurement is subject to the influence of the nonlinearity in the slope interval of the $I_1(0,u,0)$ curve, the disturbance in the intensity of the light source, environmental disturbances, etc. In a SATCM, the intensity curve, $I(0,u)$, obtained through heterodyne subtraction is used for measurement of the dimensions of 3D microstructures. It is seen from Fig.3 that a SATCM works in the range of $I(0,u) \geq 0$ when it is used for measuring the dimensions of 3D microstructures, and in comparison with $I_1(0,u,0)$, the linearity and resolution of $I(0,u)$ are significantly improved. In a SATCM, $I(0,u)$ is obtained through pairwise heterodyne subtraction of $I_1(0,u,0)$, $I_2(v,u,-u_M)$, and $I_3(v,u,+u_M)$, and the effect of variations in the intensity of the SATCM, the reflectivity of the surface of the object, and environmental factors on the intensity signals $I(0,u)$ and $I_{\mathrm{C}}(0,u)$ are dramatically reduced, and the anti-environmental interference capability of the SATCM is thus significantly improved.

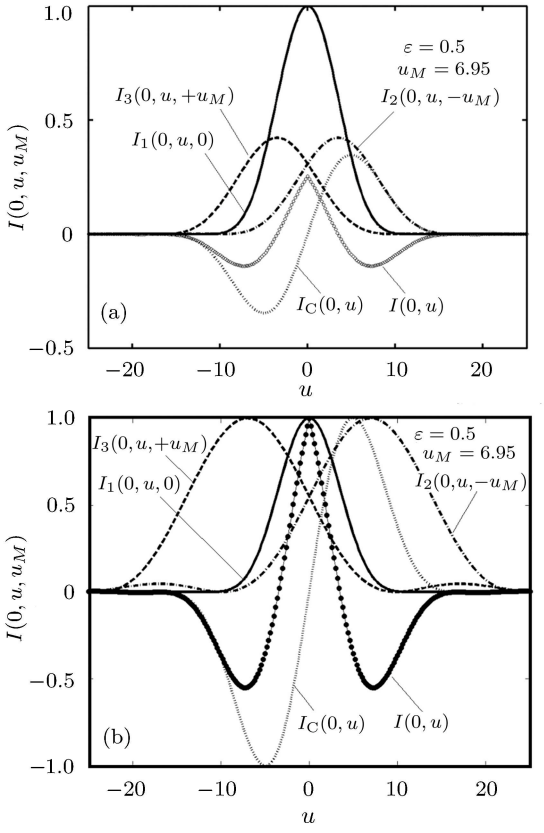


Fig.3. Simulated axial intensity curves of the SATCM. (a) Axial intensity response. (b) Normalized axial intensity response.

Figure 4(a) shows the lateral response curves

$I_1(v,0,0)$ and $I(v,0)$ for $\varepsilon = 0.5$ and $u_M = \pm 6.95$, and Fig.4(b) shows their normalized lateral response curves. The SATCM works in the range $I(v,u) \geq 0$ when it is used for the measurement of the dimensions of 3D microstructures, and it is seen from Fig.4(b) that the slope of the bevel interval in curve $I(v,0)$ is larger than that in curve $I_1(v,0,0)$ in the measurement range (i.e. SATCM lateral resolution is improved).

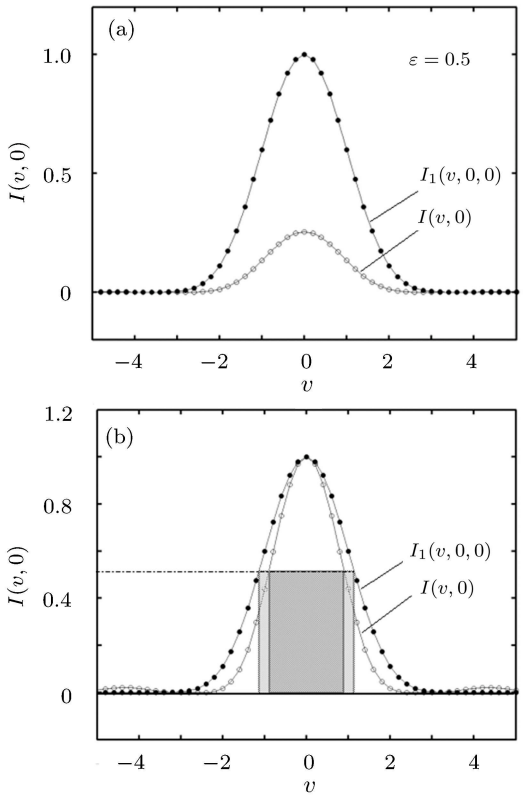


Fig.4. Simulated lateral intensity curves of SATCM. (a) Lateral intensity response. (b) Normalized lateral intensity response.

3. Experiments and analysis

3.1. Axial resolution

A SATCM experimental setup is shown in Fig.1. Its objective lens used is a 60×0.85 microscope lens, and the pinholes are 10 μm in diameter. The BOE is a diffractive optical element with 16 levels; the wavelength of the beam incident on the BOE is $\lambda = 632.8$ nm, and the maximal diameter of the incident beam is 4.3 mm. BOE can shape the incident beam into an annular beam with an inner radius of 0.435 mm and an outer radius of 1.737 mm. The BOE fitted with an adjustable diaphragm can shape a beam into an annular beam with an inner diameter of 0.87 mm and an outer diameter of less than 3.45 mm, which is required for super-resolution. The emitting annular laser beam has an inner diameter of 0.87 mm and an outer diameter of 1.8 mm, with $\varepsilon \approx 0.5$, when the diameter of the adjustable diaphragm is set at 1.8 mm. The object to be measured is a gauge block, which can be moved using a movable platform in the axial direction of the SATCM, and its movement is measured using a HP5529A laser heterodyne interferometer. Figure 5(a) shows the actual intensity curves, $I_1(0,z,0)$, $I_2(0,z,-M)$, and $I_3(0,z,+M)$, and the axial intensity curves, $I_C(0,z)$ and $I(0,z)$, obtained through pairwise heterodyne subtraction of $I_1(0,z,0)$, $I_2(0,z,-M)$, and $I_3(0,z,+M)$. Figure 5(b) shows the normalized axial intensity curves of $I_1(0,z,0)$ and $I(0,z)$.

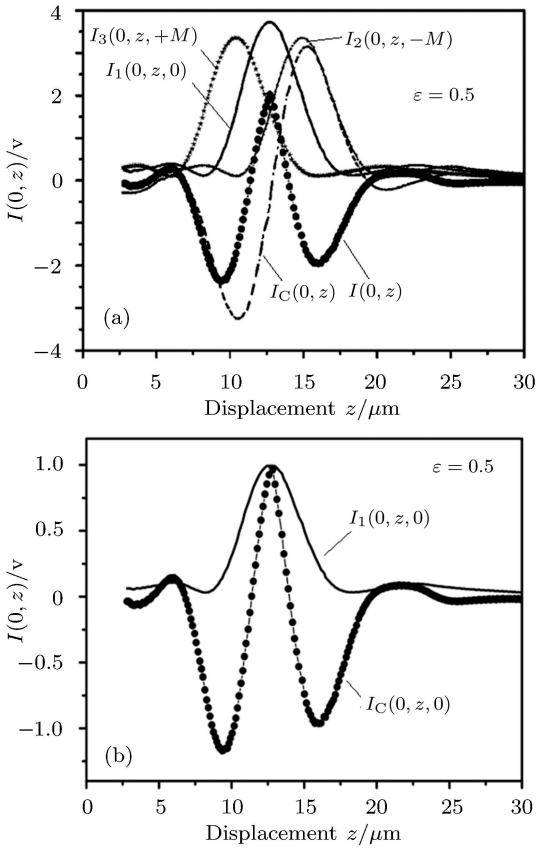


Fig.5. The axial intensity curves of the SATCM. (a) Axial intensity curve. (b) Normalized axial intensity curve.

It is seen from Fig.5(b) that the slope in the bevel interval of the curve $I(0,z)$ is obviously larger than that of the curve $I_1(0,z,0)$ in the range of $I(0,z) \geq 0$, and that the linearity of the two slope intervals of the curve $I(0,z)$ is better than that of the curve $I_1(0,z,0)$ and the side lobe has a smaller effect on the measurements in the range $I(0,z) \geq 0$.

Figure 5(a) indicates that the measurement range of the single-slope linear interval of the SATCM is 2 μm and the corresponding voltage is 5 V. When the platform moves about 2 nm, the corresponding variation in the SATCM voltage is about 5 mV and the stability of the voltage is better than 2 mV/min. It is therefore concluded from the analysis that the effective axial resolution of the experimental SATCM system is about 1 nm.

In Fig.5(a), compared with $I_1(0, z, 0)$, the linear range of the intensity curve $I_C(0, z)$ is extended, the resolution and linearity of the curve $I_C(0, z)$ are improved, and there is an absolute measurement zero in the curve $I_C(0, z)$. All these measurements are in good agreement with the results of the simulations and theoretical analyses mentioned previously.

3.2. Lateral resolution

The improved lateral resolution of SATCM is further verified by measuring the skip distance of the standard step in the lateral direction.

The standard step measurements obtained using a Dimension3100 atomic force microscope (AFM) (DI Company) are shown in Fig.6(a), where the vertical distance between two identification points is about 118.23 nm and the horizontal skip distance of the step is 0.1367 μm. Figure 6(b) shows the lateral scanning curve measured using the SATCM with NA = 0.85 and $\varepsilon = 0.50$, where the voltage corresponding to the vertical skip distance is 295 mV, and the horizontal skip distance of the step is about 0.268 μm. The lateral resolution of the SATCM is better than 0.2 μm if the skip distance of the step itself is 0.1367 μm. It can therefore be concluded that the SATCM has an improved lateral resolution compared with CMs, and the improvement increases as ε increases. In general, the reduction in the axial resolution of the CM caused by the choice of ε should be taken into consideration when selecting ε.

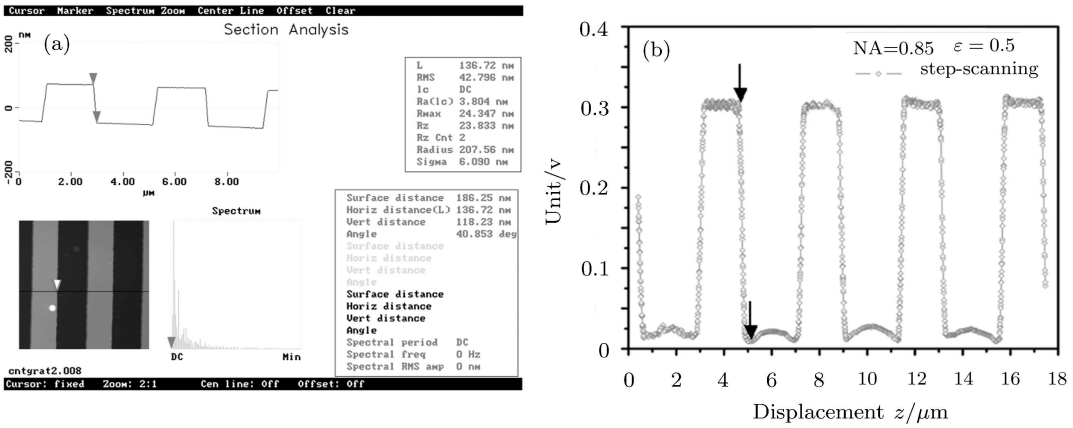


Fig.6. Measurements of steps in the lateral section. (a) Standard step obtained by AFM scanning. (b) Standard step established by the SATCM.

4. Conclusions

Theoretical analyses and preliminary experiments indicate that a SATCM constructed based on the lateral super-resolution of a shaped annular beam and the higher axial resolution of the tri-heterodyne confocal microscopy has a stronger anti-environmental-interference capability. It can

1. suppress the common-mode interference caused by variations in the intensity of the light source, the reflectivity of the surface of the object, the ambient light, the ambient temperature, and environmental vibrations, and significantly improve the anti-environmental interference capability of CMs;

2. improve the spatial resolution of CMs and achieve a lateral resolution better than 0.2 μm and an axial resolution of about 1 nm; and

3. improve the linearity of the axial response of CMs and thereby its accuracy of measurement.

SATCM provides a new imaging approach for obtaining good anti-environmental- interference capability required for optical microscopy.

References

[1] Sheppard C J R and Matthews H J 1988 *Mod. OPT* **35** 145

[2] Lee C H and Wang J P 1997 *Optics Comm.* **35** 233

[3] Udupa G, Singaperumal M, Sirohi R S and Kothiyal M P 2000 *Meas. Sci. Technol.* **11** 305

[4] Udupa G, Singaperumal M, Sirohi R S and Kothiyal M P 2000 *Meas. Sci. Technol.* **11** 315

[5] Yang L S, Wang G Y, Wang J G and Xu Z Z 2000 *Meas. Sci. Technol.* **11** 1786

[6] Zhao W Q, Chen S S and Feng Z D 2006 *Acta Phys. Sin.* **55** 3363 (in Chinese)

[7] Zhao W Q, Tan J B, Qiu L R and Zou L M 2005 *Meas. Sci. Technol.* **16** 499

[8] Sheppard C J R 1995 *OPTIK* **99** 32

[9] Wilson T and Hewlett S J 1991 *Opt. Lett.* **16** 1062

[10] Gauderon R and Sheppard C J R 1998 *Bioimaging* **6** 126

[11] De Juana D M, Oti J E, Canales V F and Cagigal M P 2003 *Opt. Lett.* **28** 607

[12] Zhao W Q, Qiu L R and Feng Z D 2006 *Opt. Express* **14** 7024

[13] Xiao F R, Yuan J H, Wang G Y and Xu Z Z 2004 *Acta Phys. Sin.* **53** 1731 (in Chinese)

[14] Martinez-Corral M, Andres P, Zapata-Rodriguez C J and Kowalczyk M 1999 *Optics Comm.* **165** 267

[15] Liu L, Deng X Q, Wang G Y and Xu Z Z 2001 *Acta Phys. Sin.* **50** 48 (in Chinese)

[16] Deng X Q, Wang G Y and Xu Z Z 2001 *Chin. J. Lasers* **28** 459

[17] Zhao W Q 2003 *Key Measurement Technique for Ultra-precision Discontinuous Cylindrical Form* (Doctor Degree Dissertation, Harbin: Harbin Institute of Technology) p99